Time-Averaged Subspace Methods for Radar Clutter Texture Retrieval

Fulvio Gini, *Senior Member, IEEE*, Georgios B. Giannakis, *Fellow, IEEE*, Maria Greco, *Member, IEEE*, and G. Tong Zhou, *Senior Member, IEEE*

***Abstract*—Subspace approaches have become popular in the last two decades for retrieving constant amplitude harmonics observed in white additive noise because they may exhibit superior resolution over the FFT-based methods, especially with short data records and closely spaced harmonics. We demonstrate here that MUSIC and ESPRIT methods can also be applied when the harmonics are corrupted by white or wideband multiplicative noise. The application context is the retrieval of texture information from high resolution and low grazing angle radar clutter data affected by wideband colored speckle that is modeled as complex multiplicative noise. Texture information is fundamental for clutter cancellation and constant false alarm rate (CFAR) radar detection. A thorough numerical analysis compares the two subspace methods and validates the theoretical findings.**

***Index Terms*—Clutter cancellation, frequency estimation, high-resolution radar, multiplicative noise, MUSIC and ESPRIT methods, radar clutter, texture retrieval.**

I. Introduction and Problem Statement

HARMONIC retrieval in the presence of additive noise has been a classical signal processing problem for about a century. Recently, however, it has been realized that multiplicative noise may also appear in certain harmonic retrieval applications. Multiplicative noise shows up in radar imaging due to the presence of speckle noise [4], [20], [33]. It is also encountered in weather radar and underwater acoustic applications, where the multiplicative noise could be due to the fluctuation of the medium [38]. Lightwave signals for digital communications, amplitude-modulated signals, and fading communication channels also comply with the multiplicative noise model [10], [12], [13].

In this paper, the focus is on a radar application: the estimation of the sea clutter texture as sensed by a high-resolution radar system operating at low grazing angle. Under this circumstance, the observed signal can be modeled in discrete-time as

$$I(n) = \tau(n) \cdot |x(n)|^2 = \left[A_0 + \sum_{i=1}^{M} A_i \cos(2\pi f_i n + \theta_i) \right] \cdot |x(n)|^2 \quad n = 0, 1, \ldots, N-1 \tag{1}$$

with the following assumptions.

a1) A_is are deterministic positive constants.
a2) θ_is are deterministic constants in $[-\pi, \pi)$.
a3) f_is are distinct and nonzero constants in $(-0.5, 0.5]$.
a4) Process $x(n)$ is complex valued, stationary, and zero-mean.

The only constraint that is posed on $\{f_i\}_{i=1}^{M}$, $\{A_i\}_{i=0}^{M}$, and $\{\theta_i\}_{i=1}^{M}$ is that they produce $\tau(n) \geq 0$ for every n. Motivation for the use of model (1) is detailed in Section II. Given $\{I(n)\}_{n=0}^{N-1}$, we wish to retrieve $\tau(n)$, which amounts to estimating $\{f_i\}_{i=1}^{M}$, $\{A_i\}_{i=0}^{M}$ and $\{\theta_i\}_{i=1}^{M}$.

Since the mean of $|x(n)|^2$ is nonzero, the cyclic mean of (1), i.e., the normalized Fourier transform of $I(n)$, can be used to estimate the frequencies f_i [9]. The limitation, however, is that frequencies separated less than $1/N$ cannot be resolved [28, p. 264]. This motivates us to study subspace methods [28, Sec. 9.7], which have not been applied to the random amplitude model in (1). We prove in this paper that MUSIC and ESPRIT methods are capable of retrieving harmonics in the presence of white or colored wideband multiplicative noise with unknown spectral density as well.

The organization of the paper is as follows. In Section II, we introduce the radar problem that motivates the use of signal model (1). In Section III, we briefly review the concept of time-averaging statistics for mixed processes, and then, we use this concept to formulate MUSIC and ESPRIT for harmonics observed in *white* multiplicative noise. The use of subspace methods for retrieving harmonics in wideband colored multiplicative noise is also discussed. Simulation examples are provided in Section IV to illustrate the two estimation algorithms and their ability to retrieve clutter texture information from intensity data. Finally, conclusions are drawn in Section V.

II. High-Resolution Radar Sea Clutter Model

The most popular statistical model in the radar literature for high-resolution and low grazing angle sea clutter is the *compound-Gaussian* model [6], [30], [34], [35]. According to this model, samples of the complex envelope of the sea clutter process are expressed as the product between two components: $z(n) = \sqrt{\tau(n)}x(n)$. Factor $x(n) = x_I(n) + jx_Q(n)$ is a complex Gaussian process, which is usually called the

Manuscript received May 22, 2000; revised June 4, 2001. The work of F. Gini and M. Greco was supported by the Italian Space Agency (ASI) through Project ZODA900167. The associate editor coordinating the review of this paper and approving it for publication was Dr. Olivier Besson.

F. Gini and M. Greco are with Department of Information Engineering, University of Pisa, Pisa, Italy (e-mail: f.gini@ing.unipi.it; m.greco@ing.unipi.it).

G. B. Giannakis is with Department of Electrical and Computer Engineering, University of Minnesota, Minneapolis, MN 55455 USA (e-mail: georgios@ece.umn.edu).

G. T. Zhou is with School of Electrical and Computer Engineering, Georgia Institute of Technology, Atlanta, GA 30332-0250 USA (e-mail: gtz@ece.gatech.edu).

Publisher Item Identifier S 1053-587X(01)07046-5.

speckle, and accounts for local backscattering; $x_I(n)$ and $x_Q(n)$ are the in-phase (I) and quadrature (Q) components that are assumed to satisfy $E\{x_I(n)\} = E\{x_Q(n)\} = 0$ with $E\{x_I^2(n)\} = E\{x_Q^2(n)\} = 1/2$; thus, the speckle power is $\sigma_X^2 = E\{|x(n)|^2\} = 1$. Factor $\tau(n)$ is a non-negative real random process, which is usually called *texture*; it describes the underlying mean power level of the data. Due to their different physical origin, these two components present different correlation lengths. For X-band high-resolution data, the speckle correlation length was measured to be on the order of tens of milliseconds, while that of the texture was on the order of seconds [8]. Although many hypotheses have been formulated and tested on measured sea clutter data, they pertain to the one-dimensional (1-D) probability density function (PDF) of the texture and of the clutter amplitude [2], [5], [8], [19], [36]. In fact, because of its long correlation time, the texture has been, so far, considered constant within each radar coherent processing interval (CPI), changing according to a given PDF from one CPI to the next, that is, $z(n) = \sqrt{\tau}x(n)$ for $n = 0, 1, \ldots, N-1$; thus, $\mathbf{z} = [z(0)z(1)\cdots z(N-1)]^T$ is a *spherically invariant random vector* (SIRV) [31], [35]. Conditioned on a given value of τ, the complex data vector $\mathbf{z}$ is Gaussian distributed. Thanks to this property, this model is mathematically tractable and has gained popularity in the radar literature [11], [14], [15], [30], [34]. However, there is a prominent interest to model the texture as a process, in order to predict its behavior in time intervals greater than a CPI, for clutter cancellation and constant false alarm rate (CFAR) detection purposes [3], [25], [26].

For ocean imaging, it is common practice to analyze and plot samples of the intensity of the radar echo, that is, the modulo squared of the complex envelope samples, which are sometimes incoherently integrated over a small space-time window, to highlight the local power and to reduce the speckle effect. If the sea is fully developed, the characteristic periodic wave structure with alternating crests and troughs is clearly visible in the range-time or range-azimuth intensity maps, particularly in VV polarization [26], [29]. For the compound-Gaussian sea radar clutter, the intensity is given by $I(n) = |z(n)|^2 = \tau(n)|x(n)|^2$. Due to their different correlation lengths, the texture and the speckle have been usually separated using lowpass filtering [8], [22]; in particular, the texture has been estimated (nonparametrically) by means of a moving-window filter of length $L+1$ as

$$\hat{\tau}(n) = \frac{1}{L+1}\sum_{k=n-L/2}^{n+L/2} I(k) \cong \tau(n)\frac{1}{L+1}\sum_{k=n-L/2}^{n+L/2}|x(k)|^2 = \tau(n)\hat{\sigma}_X^2. \quad (2)$$

In order for the approximation in (2) to be valid, parameter L should be such that $L_X \ll L \ll L_\tau$, where L_X and L_τ are the speckle and texture correlation lengths, respectively. The term $\hat{\sigma}_X^2$ in (2) represents the sample estimate of the speckle power whose actual value is one. When the speckle is Gaussian distributed, $\hat{\tau}(n)$ represents the maximum likelihood estimate of $\tau(n)$ given the $L+1$ data samples $\{I(k);\ n - L/2 \le k \le n+L/2\}$. Note that in order to choose the value of L, the speckle and texture correlation lengths L_X and L_τ should be known, at least approximately. A method for estimating them from measured clutter data is reported in [8] and employed in [16].

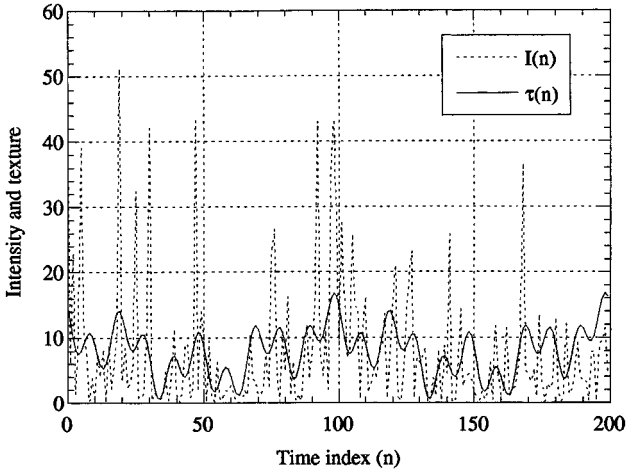

Fig. 1. Clutter intensity and texture versus time; $\rho_X = 0.1$, SNR $= -7.59$ dB, $\text{SNR}_1 = \text{SNR}_2 = \text{SNR}_3 = -15.37$ dB.

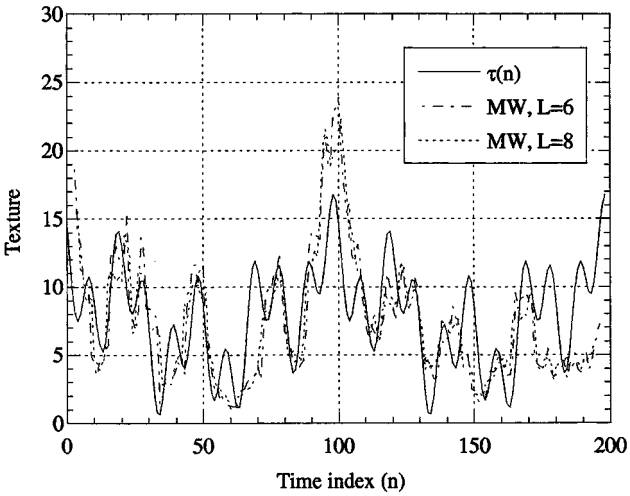

Fig. 2. Texture retrieved by means of the moving window (MW) estimator; $\rho_X = 0.1$ SNR $= -7.59$ dB, $\text{SNR}_1 = \text{SNR}_2 = \text{SNR}_3 = -15.37$ dB.

We model here the non-negative sea clutter texture as a sum of M cosinusoids and a constant term

$$\tau(n) = A_0 + \sum_{i=1}^{M} A_i \cos(2\pi f_i n + \theta_i) \quad (3)$$

so that (1) is obtained. Fig. 1 depicts a realization of $\tau(n)$ and $I(n)$ in the presence of complex Gaussian distributed speckle with Gaussian-shaped power spectral density (PSD) and with parameters given in *Example 1*. In Fig. 2, we plot the estimate of $\tau(n)$, obtained by means of the moving window (MW) estimator of (2) for $L = 6$ and $L = 8$; it is evident that the estimation accuracy is not satisfactory.

Under a1)–a4), $I(n)$ in (1) is (almost) cyclostationary[1] [7], [9], [12]. The presence of cyclostationarity in the sea clutter has

[1]Cyclostationary processes are those whose statistics are periodic functions of time. Almost, here, refers to the fact that these periods may not be integers as required by our discrete-time framework.

been already documented theoretically by Conte and Longo in [6] and empirically by Haykin and Thompson in [21]. Starting from the empirical evidence that high-resolution and low grazing angle sea clutter is cyclostationary, due to the periodic structure of the sea surface [1], [27], [32], we model the texture component of the clutter as the superposition of real cosines with unknown frequencies, amplitudes, and phases. Model (3) has been also validated by processing measured high-resolution sea clutter data in [17] and [18].

Remark 1: Estimator (2) implicitly assumes that $\tau(n) = A_0$ on a small time-window of size $L+1$ and attempts to estimate the clutter power A_0 by making use of $L+1$ samples only (with $L \ll N$). This estimate is updated at each time instant because $\tau(n)$ is locally constant, but the value of this constant changes (slowly) with time during the observation interval of length N. It is worth stressing that the estimator in (2) does not make any attempt to model the time-variation of the texture, i.e., it is a nonparametric estimator. In (3), we model the texture time variation by means of M cosinusoids, and we expect that by making use of this additional information, we can improve on the MW estimator of (2), and most importantly, we can predict its behavior outside the observation interval. Another advantage of the subspace methods to be developed in this paper is that they do not require knowledge of the speckle and texture correlation lengths. In the next sections, we show how this improvement can be obtained.

Remark 2: In (1) and subsequent analyses, we do not consider the contribution of additive thermal noise, mainly for two reasons: i) In the radar application described in Section II, the thermal noise is negligible relative to the clutter power at least for polarizations VV and HH [8], [16]; ii) we are interested in the multiplicative noise effect, which usually affects estimation accuracy more than the additive noise (the multiplicative noise is responsible for the well-known "floor" effect in estimation and detection performance). Due to lack of space, we do not include here numerical results for small clutter-to-thermal noise power ratio; however, there is no theoretical problem in including additive thermal noise to our analysis.

III. Time-Averaged Statistics and Time-Averaged Subspace Methods

First, we stress that although different realizations of the clutter process may have independent and identically distributed (i.i.d.) phases uniformly distributed in $[-\pi, \pi)$, in the clutter time series analysis, only a single record is often available. Moreover, aiming at clutter cancellation and target detection, we want to retrieve $\tau(n)$ only for the specific realization under observation, possibly on a time interval greater than that used for its estimation. Therefore, assumptions a1)–a3) are reasonable, and the model in (1) is well motivated.

As a consequence of the deterministic phase assumption a2), the process $I(n)$ is nonstationary, i.e., its statistics change with time. Ljung's unified framework for deterministic plus random (thus mixed) processes is appropriate for treating single record (non)stationary processes [23, Sect. 2.3]. Let $f(n)$ be a generally mixed process. The time-averaged expectation is denoted with overbar and is defined as

$$\overline{E}\{f(n)\} \triangleq \lim_{N\to\infty} \frac{1}{N} \sum_{n=0}^{N-1} E\{f(n)\} \tag{4}$$

if such a limit exists. Note that $\overline{E}\{\cdot\}$ is always time-independent. Two special cases of interest arise here. When $f(n)$ is purely deterministic, the $E\{\cdot\}$ drops: $\overline{E}\{f(n)\} = \lim_{N\to\infty} N^{-1} \sum_{n=0}^{N-1} f(n)$; when $f(n)$ is stationary, time averaging has no effect: $\overline{E}\{f(n)\} = E\{f(n)\}$. Within this framework, we define the time-averaged autocorrelation function (ACF) of a generally complex and mixed process $z(n)$ as

$$\overline{m}_{2z}(l) \triangleq \overline{E}\{z(n)z^*(n+l)\}. \tag{5}$$

The natural estimator of (5) from the data $\{z(n)\}_{n=0}^{N-1}$ is given by

$$\hat{\overline{m}}_{2z}(l) = \frac{1}{N} \sum_{n=0}^{N-l-1} z(n)z^*(n+l) \tag{6}$$

and can be shown to be asymptotically unbiased and mean square sense consistent for the cyclostationary process (1) [7], [38].

We now show that subspace methods, such as MUSIC and ESPRIT, are applicable rigorously and without approximation for estimating the cosinusoidal frequencies in the presence of *white* multiplicative noise. Later on, in Section IV, we show by numerical examples that they still perform well in the colored wideband multiplicative noise scenario so that they can be used to retrieve texture information from clutter data in the presence of wideband colored speckle. However, before we proceed, we wish to point out that a harmonic-in-multiplicative-noise process is different from a narrowband process, and hence, the analysis that follows does not apply directly to the former. A narrowband process $y(n)$ satisfies $y(n+l) \doteq y(n)\exp(j2\pi f_c l)$, where f_c is the carrier frequency assumed to be much greater than the bandwidth of $y(n)$. At first sight, the right-hand side of the last equation looks like a random amplitude harmonic, but in fact, it is not, since the complex exponential is not a function of n [compare with (1)].

Consider now the real cyclostationary process $I(n)$ of (1). The time-averaged ACF of $I(n)$ is given by

$$\begin{aligned}\overline{m}_{2I}(l) &= \overline{E}\{I(n)I(n+l)\} \\ &= \left[A_0^2 + \tfrac{1}{2}\sum_{i=1}^{M} A_i^2 \cos(2\pi f_i l)\right] \\ &\quad \cdot E\left\{|x(n)|^2 |x(n+l)|^2\right\}. \end{aligned} \tag{7}$$

Under the Gaussianity assumption for the speckle [6], [8], [30], [34], we obtain

$$\begin{aligned}\overline{m}_{2I}(l) &= \left[A_0^2 + \tfrac{1}{2}\sum_{i=1}^{M} A_i^2 \cos(2\pi f_i l)\right] \\ &\quad \cdot \left[1 + 4R_{X_I}^2(l) + 4R_{X_I X_Q}^2(l)\right] \end{aligned} \tag{8}$$

where $R_{X_I}(l)$ ($R_{X_Q}(l)$) is the ACF of the I (Q) component, and $R_{X_IX_Q}(l)$ is the cross-correlation between the I and Q components. It holds true that $R_{X_I}(l) = R_{X_Q}(l)$. If the speckle is white noise, (8) reduces to

$$\overline{m}_{2I}(l) = A_0^2 + \tfrac{1}{2}\sum_{i=1}^{M} A_i^2 \cos(2\pi f_i l) + \left[A_0^2 + \tfrac{1}{2}\sum_{i=1}^{M} A_i^2\right]\delta(l). \tag{9}$$

In order to estimate $\{f_i\}_{i=1}^M$, it is useful to estimate A_0 first and remove its contribution, i.e., the line at zero frequency, from the data. For this purpose, define the new data as $Y(n) = I(n) - \overline{E}\{I(n)\} = I(n) - A_0$. The mean-averaged ACF of the new data $Y(n)$, in the general case of colored Gaussian speckle, is given by

$$\begin{aligned}\overline{m}_{2Y}(l) &= \overline{m}_{2I}(l) - A_0^2 \\ &= \tfrac{1}{2}\sum_{i=1}^{M} A_i^2 \cos(2\pi f_i l) + 4\left(R_{X_I}^2(l) + R_{X_IX_Q}^2(l)\right) \\ &\quad \cdot \left[A_0^2 + \tfrac{1}{2}\sum_{i=1}^{M} A_i^2 \cos(2\pi f_i l)\right].\end{aligned} \tag{10}$$

Note that the time-averaged autocorrelation in (10) has the same structure as the autocorrelation of a stationary process composed by the superposition of constant amplitude harmonics with i.i.d. uniformly distributed phases and colored additive noise. For white speckle, i.e., white multiplicative noise, (10) reduces to

$$\overline{m}_{2Y}(l) = \tfrac{1}{2}\sum_{i=1}^{M} A_i^2 \cos(2\pi f_i l) + \left[A_0^2 + \tfrac{1}{2}\sum_{i=1}^{M} A_i^2\right]\delta(l). \tag{11}$$

Interestingly, in this case, the time-averaged autocorrelation has the same structure as the autocorrelation of the stationary process

$$u(n) = \sum_{i=1}^{M} A_i \cos(2\pi f_i n + \phi_i) + v(n) \tag{12}$$

where the ϕ_is are i.i.d. uniformly distributed in $[-\pi, \pi)$, and $v(n)$ is white noise with variance $\sigma_v^2 = A_0^2 + \sum_{i=1}^{M} A_i^2/2$. It is exactly this property that allows us to employ subspace methods that were originally proposed for estimating harmonics embedded in additive white noise, as well as for retrieving harmonics affected by multiplicative white noise.

To proceed, define the data vector $\mathbf{y} = [Y(0)\ \ Y(1)\ \ \cdots\ \ Y(K)]^T$, where $K \geq 2M$, and the autocorrelation matrix $\mathbf{R}_Y = \overline{E}\{\mathbf{y}\mathbf{y}^T\}$. The $(K+1)\times(K+1)$ matrix $\mathbf{R}_Y$ is real, symmetric, and Toeplitz. Analogous to common MUSIC and ESPRIT analyses, it is easy to verify that $\mathbf{R}_Y$ can be decomposed as $\mathbf{R}_Y = \mathbf{S}\mathbf{D}\mathbf{S}^H + \sigma_\nu^2\mathbf{I}$, where $\mathbf{S} = [\mathbf{e}(f_{-M})\ \cdots\ \mathbf{e}(f_{-1})\ \mathbf{e}(f_1)\ \cdots\ \mathbf{e}(f_M)]$ is the $(K+1)\times(2M)$ so-termed steering matrix $\mathbf{e}(f_i) \triangleq [1\ \ e^{-j2\pi f_i}\ \ \cdots\ \ e^{-j2\pi f_i K}]^T$, $\mathbf{D} = \text{diag}\{[A_M^2\ \cdots\ A_1^2\ A_1^2\ \cdots\ A_M^2]\}/4$, $\mathbf{I}$ is the identity matrix, and $\sigma_\nu^2 \triangleq A_0^2 + \sum_{i=1}^{M} A_i^2/2$ is the (self-) noise power. Therefore, eigendecomposition is performed on the time-averaged autocorrelation matrix, the same way that is applied to constant amplitude harmonics. This shows that we can apply subspace methods, like MUSIC and ESPRIT, for estimating $\{f_i\}_{i=1}^M$ from the clutter intensity data when the speckle is white. We refer to [28, Ch. 9] for subsequent development of MUSIC and ESPRIT.

Matrix $\hat{\mathbf{R}}_Y$ is built from the estimates of $\overline{m}_{2Y}(l)$ for $-K \leq l \leq K$, which in turn are obtained as

$$\hat{\overline{m}}_{2Y}(l) = \frac{1}{N}\sum_{n=0}^{N-l-1}\left[I(n) - \hat{A}_0\right]\cdot\left[I(n+l) - \hat{A}_0\right] \tag{13}$$

where $\hat{A}_0 = \sum_{n=0}^{N-1} I(n)/N$ is the sample mean of the intensity data (we do not know A_0 so we use an estimate of it). $\hat{A}_0$ is an unbiased and mean square sense (m.s.s.) consistent estimator of A_0, and $\hat{\overline{m}}_{2Y}(l)$ is an asymptotically unbiased and m.s.s. consistent estimator of $\overline{m}_{2Y}(l)$ in (11). Estimates $\hat{\overline{m}}_{2Y}(l)$ and $\hat{\overline{m}}_{2I}(l)$ are related as follows:

$$\begin{aligned}\hat{\overline{m}}_{2Y}(l) &= \hat{\overline{m}}_{2I}(l) - \hat{A}_0\frac{1}{N}\sum_{n=0}^{N-l-1} I(n+l) \\ &= \hat{\overline{m}}_{2I}(l) - \hat{A}_0\left[\hat{A}_0 - \frac{1}{N}\sum_{n=0}^{l-1} I(n)\right]\end{aligned} \tag{14}$$

where $\hat{\overline{m}}_{2I}(l) = \sum_{n=0}^{N-l-1} I(n)I(n+l)/N$. As $N \to \infty$, (14) becomes $\overline{m}_{2Y}(l) = \overline{m}_{2I}(l) - A_0^2$.

In the next section, we will show by means of a thorough numerical analysis that even if MUSIC and ESPRIT have been designed for additive white noise and extended here to the case of multiplicative white noise, they work fairly well also for wideband colored multiplicative noise. The performance depends on the "memory" Q of the ACF of the multiplicative noise $|x(n)|^2$, that is, related to the value of the lag l beyond which $R_X(l)$ is negligible. If $Q \ll K$, then both the subspace algorithms "blindly" applied to the intensity data provide accurate frequency estimates. The intuition behind this surprisingly good performance is that a large-size banded Toeplitz matrix with a small "bandwidth" parameter behaves like a diagonal matrix [38].

MUSIC and ESPRIT methods provide estimates of the frequencies $\{f_i\}_{i=1}^M$. For the purpose of texture retrieval, we need the estimates of amplitudes and phases, as well. The term A_0 is estimated separately as $\hat{A}_0 = \sum_{n=0}^{N-1} I(n)/N$. To estimate $\{A_i\}_{i=1}^M$ and $\{\theta_i\}_{i=1}^M$, we use the nonlinear least squares (NLLS) method, that is, we estimate the unknown parameters as the minimizers of the following criterion:

$$g(A_i, \theta_i) = \sum_{n=0}^{N-1}\left|I(n) - \hat{A}_0 - \sum_{i=1}^{M} A_i \cos\left(2\pi\hat{f}_i n + \theta_i\right)\right|^2 \tag{15}$$

where $\hat{f}_i$ are the frequency estimates. By making use of the notation found in (16) and (17), shown at the bottom of the next page, we can verify that the vector $\boldsymbol{\beta}$, which minimizes $g(\cdot)$ in (15), is given by

$$\hat{\boldsymbol{\beta}} = (\mathbf{B}^*\mathbf{B})^{-1}\mathbf{B}^*\mathbf{y}_0 \tag{18}$$

where $\mathbf{y}_0 \triangleq [I(0) - \hat{A}_0\ \ I(1) - \hat{A}_0\ \ \cdots\ \ I(N-1) - \hat{A}_0]^T$, i.e., $\mathbf{y}_0$ is obtained from $\mathbf{y}$ by replacing A_0 with its estimate $\hat{A}_0$. Estimates $\{\hat{A}_i\}_{i=1}^M$ and $\{\hat{\theta}_i\}_{i=1}^M$ follow immediately from $\hat{\boldsymbol{\beta}}$, and the texture is then retrieved according to (3). The fact

that the texture is non-negative was imposed in the algorithm by assuming that $\hat{\tau}(n) = 0$ for those values of n for which the retrieved texture is negative, but negative $\hat{\tau}(n)$s never occurred in our simulations, which are described in the following section.

Remark 3: The usefulness of the theoretical results derived in this section is not limited to the case investigated in this paper, where the multiplicative noise $|x(n)|^2$ is common to all the cosinusoidal components. There is an abundance of literature dealing with multicomponent models, where each component is affected by multiplicative noise that is independent from that of the other components (see, e.g., [9] and [24]). In this case, the observed signal and its time-averaged autocorrelation are given by

$$I(n) = \sum_{i=1}^{M} |x_i(n)|^2 A_i \cos(2\pi f_i n + \theta_i) \tag{19}$$

and

$$\begin{aligned}\overline{m}_{2I}(l) = {} & \tfrac{1}{2} \sum_{i=1}^{M} A_i^2 \cos(2\pi f_i l) \\ & + 2\left[R_{X_I}^2(l) + R_{X_I X_Q}^2(l)\right] \\ & \cdot \sum_{i=1}^{M} A_i^2 \cos(2\pi f_i l)\end{aligned} \tag{20}$$

that has the same structure as the autocorrelation of a stationary process composed by the superposition of constant amplitude harmonics with i.i.d. uniformly distributed phases and colored additive noise. For white multiplicative noise, (20) reduces to

$$\overline{m}_{2I}(l) = \tfrac{1}{2} \sum_{i=1}^{M} A_i^2 \cos(2\pi f_i l) + \left(\tfrac{1}{2} \sum_{i=1}^{M} A_i^2\right) \cdot \delta(l) \tag{21}$$

that has the same structure as the autocorrelation of a stationary process composed by the superposition of constant amplitude harmonics with i.i.d. uniformly distributed phases and white additive noise. Therefore, we can also employ subspace methods for retrieving harmonics affected by independent multiplicative white or wideband noises.

IV. Numerical Analysis of Time-Averaged MUSIC and ESPRIT

To evaluate the estimation accuracy of time-averaged MUSIC and ESPRIT, we carried out 1000 Monte Carlo trials, generating for each trial a vector of N complex samples according to the model (1). The speckle $\{x(n)\}$ is complex Gaussian distributed with Gaussian shaped PSD. The autocorrelation sequence is

$$R_X(l) = 2R_{X_I}(l) = \rho_X^{l^2} \tag{22}$$

and $R_{X_I X_Q}(l) = 0$, where ρ_X is the one-lag speckle correlation coefficient. Note that the lower ρ_X is, the shorter the length Q of the multiplicative noise ACF will be. Under the above assumption, we find the time-averaged ACF of the new intensity data $Y(n) = I(n) - A_0$ from (10) as

$$\begin{aligned}\overline{m}_{2Y}(l) = {} & \tfrac{1}{2} \sum_{i=1}^{M} A_i^2 \cos(2\pi f_i l) \\ & + \left[A_0^2 + \tfrac{1}{2} \sum_{i=1}^{M} A_i^2 \cos(2\pi f_i l)\right] \rho_X^{2l^2}.\end{aligned} \tag{23}$$

The first sum on the right-hand side of (23) represents the contribution of the "signal" component, whereas the second one the contribution of the "noise" component. Calculating (23) at lag zero, we obtain $\overline{m}_{2Y}(0) = \sum_{i=1}^{M} A_i^2/2 + \sigma_\nu^2$, where σ_ν^2 is the term in square brackets in (23) calculated at lag $l = 0$, which was called self-noise in Section III. We define the overall signal-to-noise ratio (SNR) and the ith signal-to-noise ratio (SNR$_i$) as

$$\text{SNR} \triangleq \frac{\sum_{i=1}^{M} A_i^2/2}{\sigma_\nu^2} \quad \text{and} \quad \text{SNR}_i \triangleq \frac{A_i^2/4}{\sigma_\nu^2}. \tag{24}$$

Note that since $\sigma_\nu^2 > \sum_{i=1}^{M} A_i^2/2$, the SNR here is always smaller than 1, i.e., SNR < 0 dB. Concerning the length Q, if we define the correlation length as the value of the lag at which the sequence $\rho_X^{2l^2}$ in (23) is reduced by a factor 10^{-3}, we obtain $Q = \sqrt{1.5/\text{Log}_{10}(1/\rho_X)}$. For example, if $\rho_X = 0.9$, we find $Q \cong 6$, whereas for $\rho_X = 0.1$, we obtain $Q \cong 2$.

By Fourier transforming $\overline{m}_{2Y}(l)$ in (23), we obtain the time-averaged PSD of $Y(n)$

$$\begin{aligned}S_Y(f) = {} & \tfrac{1}{4} \sum_{i=1}^{M} A_i^2 \left[\delta(f - f_i) + \delta(f + f_i)\right] + A_0^2 S_G(f) \\ & + \tfrac{1}{4} \sum_{i=1}^{M} A_i^2 \left[S_G(f - f_i) + S_G(f + f_i)\right] \\ & |f| \le 1/2\end{aligned} \tag{25}$$

where $S_G(f)$ is a Gaussian-shaped function, symmetric around $f = 0$, and with standard deviation $\sigma_G = \pi^{-1}\sqrt{\ln(1/\rho_X)}$; the

$$\boldsymbol{\beta} = [\beta_M^* \cdots \beta_1^* \beta_1 \cdots \beta_M]^T, \quad \text{with} \quad \beta_i \triangleq \frac{A_i}{2} e^{j\theta_i} \tag{16}$$

$$\mathbf{B} = \begin{bmatrix} 1 & \cdots & 1 & 1 & \cdots & 1 \\ \vdots & \cdots & \vdots & \vdots & \cdots & \vdots \\ e^{-j2\pi\hat{f}_M(N-1)} & \cdots & e^{-j2\pi\hat{f}_1(N-1)} & e^{j2\pi\hat{f}_1(N-1)} & \cdots & e^{j2\pi\hat{f}_M(N-1)} \end{bmatrix} \tag{17}$$

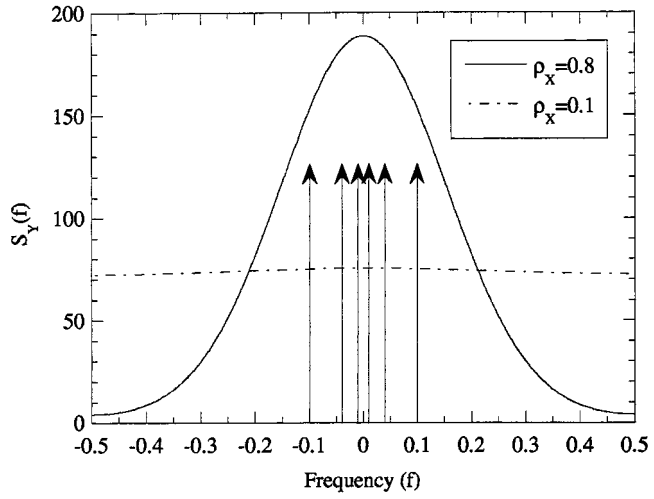

(a)

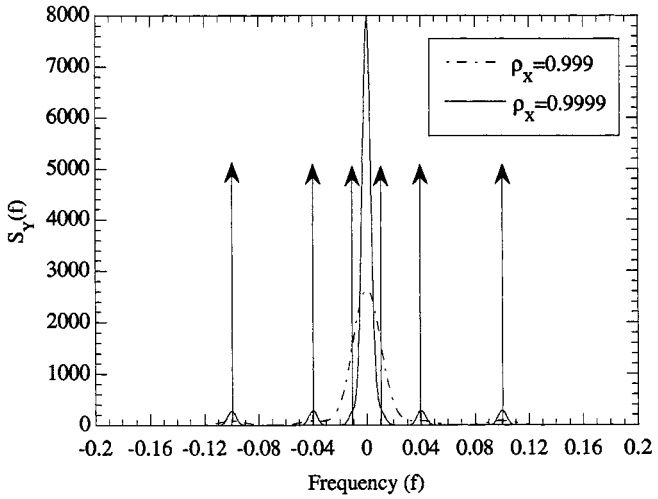

(b)

Fig. 3. (a) Time-averaged PSD of $Y(n)$ for $\rho_X = 0.1$ and 0.8. (b) Time-averaged PSD of $Y(n)$ for $\rho_X = 0.999$ and 0.9999.

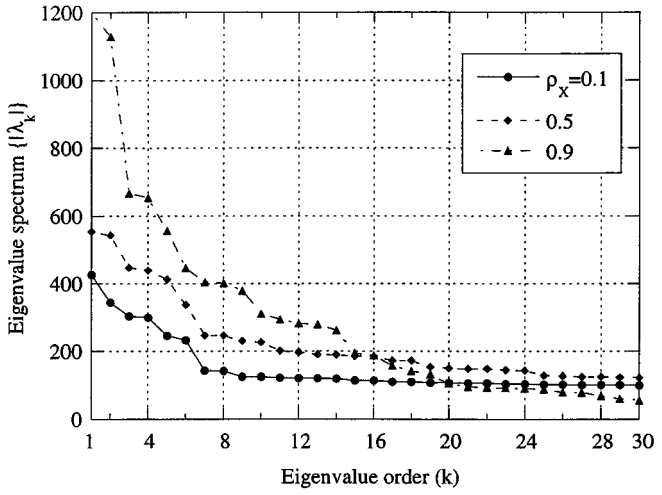

Fig. 4. Eigenvalue spectrum of the estimated correlation matrix $\hat{\mathbf{R}}_Y$; $K = 127$, SNR $= -7.59$ dB, $\text{SNR}_1 = \text{SNR}_2 = \text{SNR}_3 = -15.37$ dB.

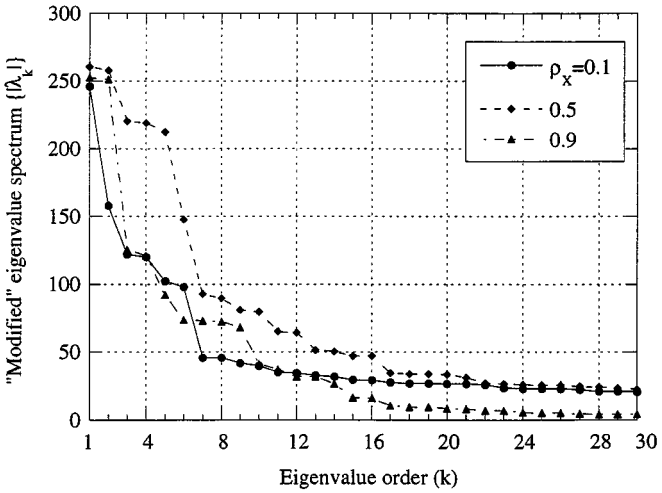

Fig. 5. Eigenvalue spectrum of the estimated modified correlation matrix; $K = 127$, $l_0 = 50$, SNR $= -7.59$ dB, $\text{SNR}_1 = \text{SNR}_2 = \text{SNR}_3 = -15.37$ dB.

greater ρ_X is, the narrower the multiplicative noise bandwidth will be. Note that $S_Y(f)$ contains both a discrete part ($2M$ lines) and a continuous part.

In agreement with previous comments, we observe that the time-averaged PSD in (25) has the same structure as the PSD of a stationary process expressed as the superposition of constant amplitude harmonics with i.i.d. uniformly distributed phases and stationary colored additive noise $v(n)$ with PSD $S_V(f) = A_0^2 S_G(f) + \sum_{i=1}^{M} (A_i^2/4)\,[S_G(f - f_i) + S_G(f + f_i)]$. Note that $S_V(f)$ is the continuous part of $S_Y(f)$, whereas the locations of the lines in $S_Y(f)$ constitute the information we want to retrieve. Plots of $S_Y(f)$ are depicted in Fig. 3(a) and (b) for different values of ρ_X, $M = 3$, $A_0 = 8$, $A_1 = A_2 = A_3 = 3$, $f_1 = 0.01$, $f_2 = 0.04$, and $f_3 = 0.1$. Parameter ρ_X affects the shape of the continuous part $S_V(f)$, which is formed by the superposition of $2M + 1$ terms with shape $S_G(f)$. The discrete part of $S_Y(f)$ is made up of $2M$ lines symmetrically located around zero. For very low values of ρ_X, $S_V(f)$ is almost flat. When ρ_X increases, the shape of $S_G(f)$ becomes narrower, and likewise for $S_V(f)$. Note that the "local" SNR for each discrete line in the spectrum changes with ρ_X in a way that depends on the shape of $S_G(f)$ as well as on the values of $\{f_i\}_{i=1}^{M}$. In Fig. 3, we observe that it decreases with ρ_X; thus, we expect estimation accuracy to get worse as ρ_X increases. When ρ_X becomes very close to one, the $2M + 1$ terms in $S_V(f)$ with the shape of $S_G(f)$ become very peaky, and $S_V(f)$ assumes a multimodal shape, as shown in Fig. 3(b). When $\rho_X \to 1$, each term tends to a delta of Dirac and the time-averaged PSD becomes purely discrete: The $2M$ lines already present plus a line at zero frequency. Therefore, when $\rho_X \cong 1$, $S_V(f)$ behaves like a useful signal, and estimation accuracy is expected to improve abruptly. To numerically evaluate the performance of the proposed time-averaged MUSIC and ESPRIT estimators, we calculated the mean square error (MSE) for a few case studies.

Example 1: Cosinusoids with Identical Amplitudes: We set $M = 3$, $N = 1024$, $A_0 = 8$, $A_1 = A_2 = A_3 = 3$, $f_1 = 0.01$, $f_2 = 0.04$, $f_3 = 0.1$, $\theta_1 = 0$, $\theta_2 = \pi/4$, and $\theta_3 = \pi/3$; as a result, we have $\text{SNR}_1 = \text{SNR}_2 = \text{SNR}_3 = -15.37$ dB, and SNR $= -7.59$ dB. As a first step, we investigate how the rank of

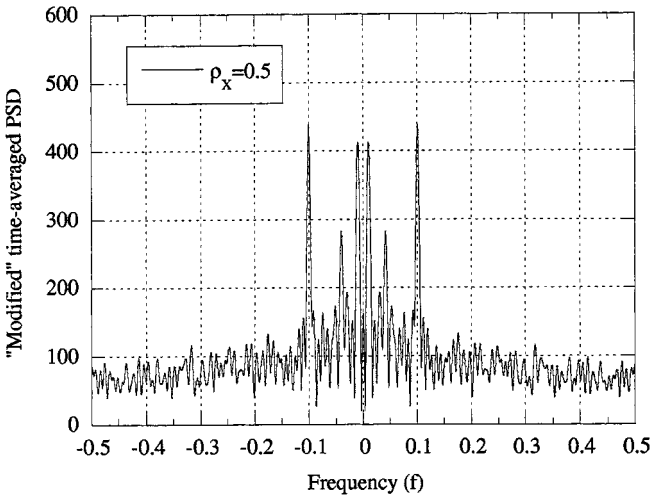

Fig. 6. Modified time-averaged power spectral density; $K = 127$, SNR $= -7.59$ dB, $\text{SNR}_1 = \text{SNR}_2 = \text{SNR}_3 = -15.37$ dB.

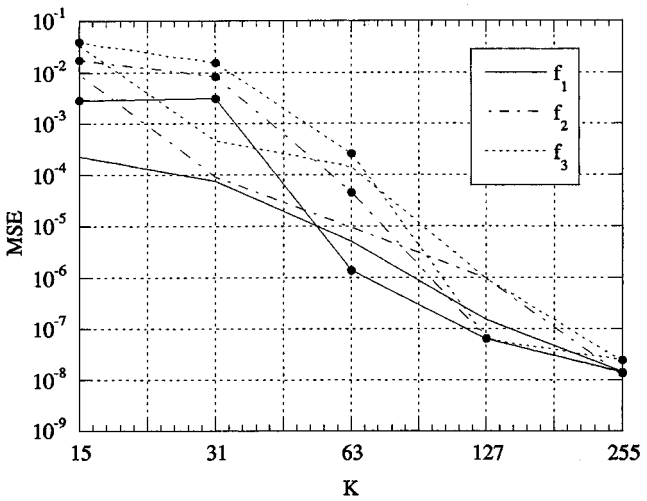

Fig. 8. Mean square frequency estimation error by means of ESPRIT (lines) and MUSIC (lines with marks •) as a function of the covariance matrix size; $\rho_X = 0.1$, SNR $= -7.59$ dB, $\text{SNR}_1 = \text{SNR}_2 = \text{SNR}_3 = -15.37$ dB.

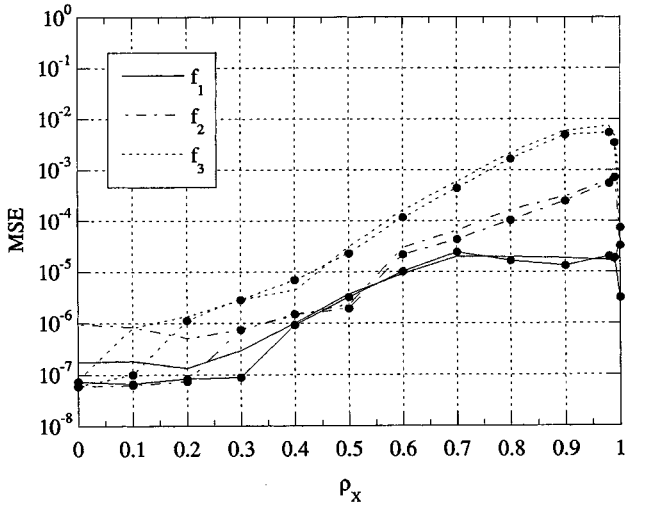

Fig. 7. Mean square frequency estimation error by means of ESPRIT (lines) and MUSIC (lines with marks •) as a function of ρ_X; $K = 127$, SNR $= -7.59$ dB, $\text{SNR}_1 = \text{SNR}_2 = \text{SNR}_3 = -15.37$ dB.

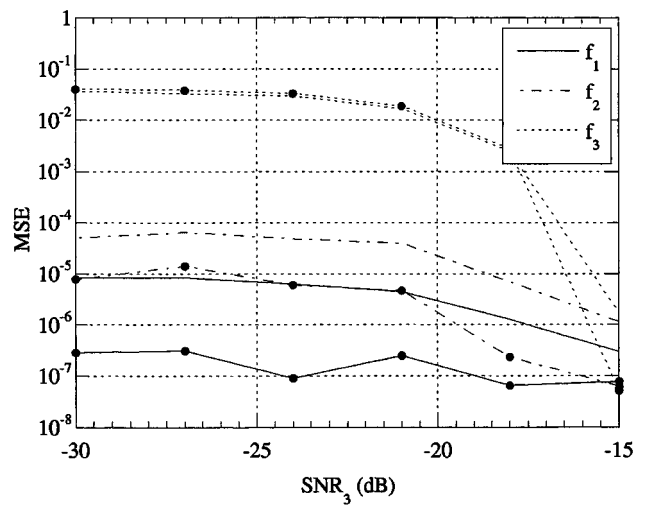

Fig. 9. Mean square frequency estimation error by means of ESPRIT (lines) and MUSIC (lines with marks •) as a function of SNR_3; $K = 127$, $\rho_X = 0.1$, $A_0 = 8$, $A_1 = A_2 = 3$.

the covariance matrix $\mathbf{R}_Y$ depends on the one-lag speckle correlation coefficient ρ_X. In the absence of multiplicative noise, we have that $\text{rank}(\mathbf{R}_Y) = 2M$. In the presence of speckle, when $\rho_X = 1$, the rank is $2M+1$; indeed, the completely correlated, nonzero-mean, multiplicative noise generates a line at zero frequency. When $\rho_X \neq 1$, we have $\text{rank}(\mathbf{R}_Y) = K + 1$, i.e., $\mathbf{R}_Y$ is full rank. In Fig. 4, we plot the first 30 eigenvalues of $\hat{\mathbf{R}}_Y$ [estimated from a single realization through (13)] for three different values of ρ_X. It is quite evident that for $\rho_X \leq 0.5$, the eigenvalues $\{\lambda_k\}$ show an abrupt decrease for $k > 2M$; thus, for wideband speckle, M can be inferred by inspecting the estimated eigenvalue spectrum. Alternatively, (23) suggests a way to get rid of (or reduce) the effect of multiplicative noise, therefore, obtaining a better estimate of M. In fact, if we calculate the correlation sequence $\overline{m}_{2Y}(l)$ for $l_0 \leq l \leq K$, with $l_0 > Q$, we get $\overline{m}_{2Y}(l) \cong \sum_{i=1}^{M} (A_i^2/2)\cos(2\pi f_i l)$. Therefore, forming the $(K - l_0 + 1) \times (K - l_0 + 1)$ "modified" autocorrelation matrix using only the values of $\overline{m}_{2Y}(l)$ for lags $l_0 \leq l \leq K$, we obtain a matrix with rank $2M$. This suggests estimating M by counting the number of dominant eigenvalues in the eigenvalue spectrum of the modified $\hat{\mathbf{R}}_Y$. In Fig. 5, we plot the first 30 eigenvalues of the modified $\hat{\mathbf{R}}_Y$. Alternatively, we may count the dominant (and symmetric) peaks in the modified time-averaged PSD obtained by Fourier transforming the sequence $\{\hat{\overline{m}}_{2Y}(l);\ l_0 \leq l \leq K\}$. In Fig. 6, we plot one estimate of the modified time-averaged PSD for $\rho_X = 0.5$; when $\rho_X \leq 0.5$, the six symmetric peaks are even more distinguishable. The curves in Figs. 5 and 6 were obtained for $l_0 = 50$ and $K = 127$. Note that $l_0 \gg Q$; in fact, for $\rho_X = 0.9$, we found $Q \cong 6$. Finally, it is worth stressing that since the time-averaged ACF in (10) and (23) has the same structure as the autocorrelation of a stationary process composed of the superposition of constant amplitude harmonics with i.i.d. uniformly distributed phases and colored additive noise, all the methods for model order determination already proposed for MUSIC in colored noise can be applied as well.

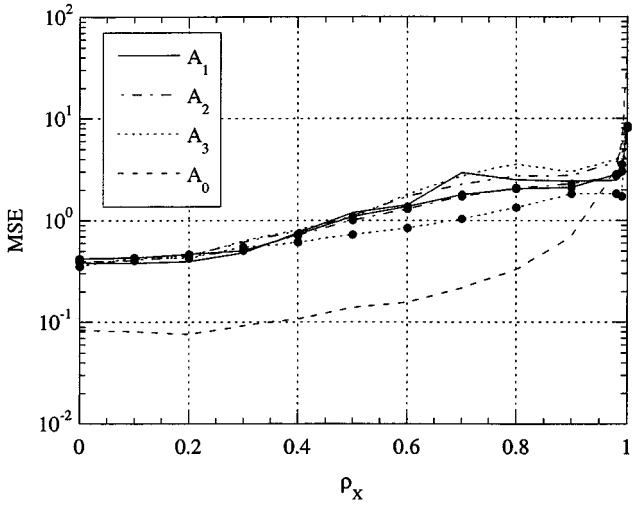

Fig. 10. Mean square amplitude estimation error by means of ESPRIT (lines) and MUSIC (lines with marks •) as a function of ρ_X; $K = 127$, SNR $= -7.59$ dB, $\text{SNR}_1 = \text{SNR}_2 = \text{SNR}_3 = -15.37$ dB.

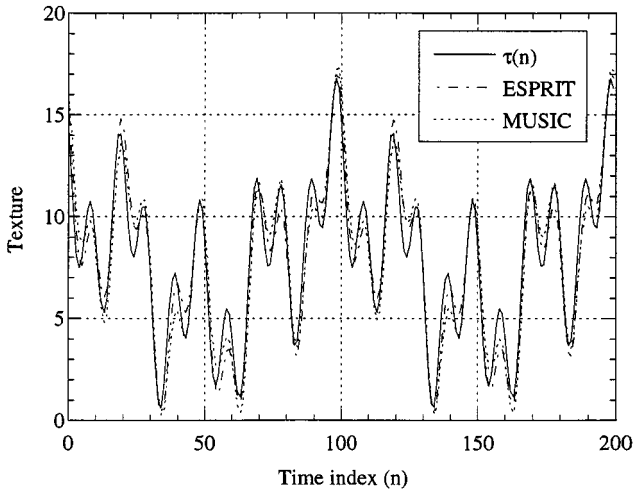

Fig. 11. Texture retrieved by means of MUSIC and ESPRIT; $K = 127, \rho_X = 0.1$, SNR $= -7.59$ dB, $\text{SNR}_1 = \text{SNR}_2 = \text{SNR}_3 = -15.37$ dB.

All the numerical results presented in the following were derived by applying MUSIC and ESPRIT as described in [28, Ch. 9] to the unmodified covariance matrix $\hat{\mathbf{R}}_Y$. However, an interesting development of the present work will be to investigate the performance of subspace methods applied to the modified $\hat{\mathbf{R}}_Y$. In Fig. 7, we report the MSE of the frequency estimates as a function of ρ_X for both MUSIC and ESPRIT methods. Lines without marks refer to ESPRIT and lines with marks (•) to MUSIC. For $K = 127$, the two methods have almost the same estimation accuracy. We also investigated the performance for $K = 31$, but the results are not reported here for lack of space. In this case, ESPRIT exhibits better performance than MUSIC for almost every value of ρ_X. Note that in Fig. 7, the lower ρ_X is, the better the estimation accuracy will be, but when $\rho_X \to 1$, estimation accuracy improves abruptly. The MSE behavior as a function of ρ_X also depends on K, on the SNRs, and on $\{f_i\}_{i=1}^M$, e.g., for $K = 31$ and the other parameters as in Fig. 7, we found that the MSE is almost constant for $\rho_X < 0.9$ (it decreases very slowly) and decreases abruptly when $\rho_X \to 1$. This abrupt decrease is also present for $K = 127$. The different behavior of the MSE versus ρ_X for $K = 31$ and $K = 127$ is probably due to the following reason. It is known that the accuracy of MUSIC and ESPRIT frequency estimates increases with increasing K (remember that $K+1$ is the size of the covariance matrix $\hat{\mathbf{R}}_Y$); hence, this value should be chosen as large as possible, but not too close to N, in order to obtain a reliable estimation of $\mathbf{R}_Y$. The variance of $\hat{\overline{m}}_{2Y}(l)$ increases both with the lag l and with the value of ρ_X (because the number of "effective" independent samples decreases with ρ_X). When $K = 31$ and $N = 1024$, the estimates $\hat{\overline{m}}_{2Y}(l)$ for the largest values of l are quite good, and thus, the effect of ρ_X on their variance is negligible; therefore, $\text{MSE}(\hat{f}_i)$ is almost constant. For $K = 127$ and $N = 1024$, estimates of $\hat{\overline{m}}_{2Y}(l)$ for the largest values of l suffer for non-negligible variance, and this variance gets worse when ρ_X increases; thus, $\text{MSE}(\hat{f}_i)$ also gets worse with ρ_X.

To further investigate the effect of K on frequency estimation accuracy, we derived the results plotted in Fig. 8, where K increases from 15 to 255, which is lower than $N/4 = 256$. We observe that for small K, ESPRIT performs better than MUSIC, whereas for large K, the situation is reversed (but for $K = 256$, they have the same performance). Moreover, it is worth observing that the MSE decreases quite abruptly when K goes from 16 to 64 and more slowly after that. In fact, for $\rho_X = 0.1$, the correlation length of the speckle is $Q \cong 2 \ll 64$, and the estimation algorithms perform like in additive white noise.

In Fig. 9, we allowed A_3 to vary while keeping A_1 and A_2 constant, leading to variable SNR_1, SNR_2, and SNR_3. Indeed, from (24), we have that $\text{SNR}_i = 0.5A_i^2/(2A_0^2+A_1^2+A_2^2+A_3^2)$. When $\text{SNR}_3 = -15.37$ dB, the three SNRs are equal. Note that the range of variation of SNR_3 has be chosen such that $\tau(n) \geq 0$ is satisfied for every n. In this range, MUSIC outperforms ESPRIT.

Curves of the MSE for the amplitude estimators in (18) are plotted in Fig. 10. The two methods exhibit almost identical performance (MUSIC is slightly better). Similar results were found for the phases. The estimates of $\{A_i\}_{i=0}^M$, $\{f_i\}_{i=1}^M$, and $\{\theta_i\}_{i=1}^M$ are then plugged into (3) to retrieve texture information. In Fig. 11, we show the true $\tau(n)$, which is the same as in Figs. 1 and 2, and $\hat{\tau}(n)$ obtained by means of ESPRIT and MUSIC. The improvement over the nonparametric WP estimator of (2) is quite evident. To quantify it, we calculate the time-averaged expectation of the squared error σ_ε^2 of the texture estimate defined as

$$\sigma_\varepsilon^2 = \overline{E}\left\{[\tau(n) - \hat{\tau}(n)]^2\right\}. \tag{26}$$

In practice, we estimated σ_ε^2 by first calculating $\hat{\sigma}_\varepsilon^2 = N^{-1}\sum_{n=0}^{N-1}[\tau(n) - \hat{\tau}(n)]^2$ for each Monte Carlo (MC) run and then averaging over the 1000 MC runs. We found $\sigma^2_{\varepsilon\text{ESPRIT}} = 0.8671$, $\sigma^2_{\varepsilon\text{MUSIC}} = 0.9928$, and $\sigma^2_{\varepsilon WP} = 22.0712$ for $L = 4$, 20.6016 for $L = 6$, and 19.4569 for $L = 8$ (see also Fig. 2). This confirms previous results.

Thus far, we have assumed that the value of M is known or that it is perfectly estimated from the eigenvalue spectrum of $\hat{\mathbf{R}}_Y$. To investigate how a wrong estimate of M affects the accuracy of texture retrieval, we assumed that the number of components in $\hat{\tau}(n)$ is $\hat{M} = 1, 3, 6, 10, 15$, whereas the actual number is still $M = 3$. For each $\hat{M}$, we estimated σ_ε^2 running

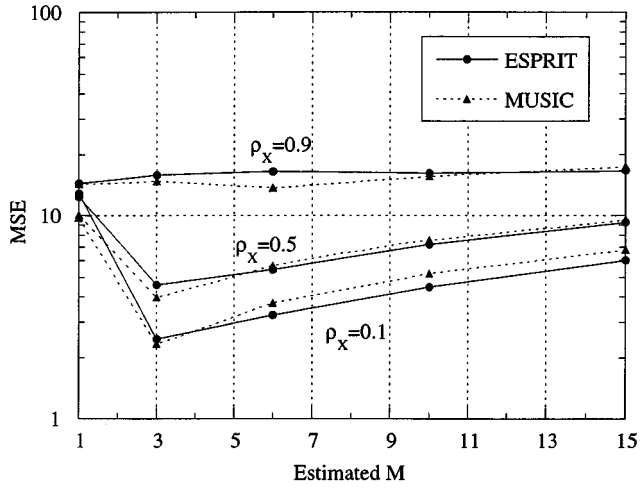

Fig. 12. Time-averaged MSE of $\hat{\tau}(n)$ retrieved by means of MUSIC and ESPRIT as a function of the estimated value of M.

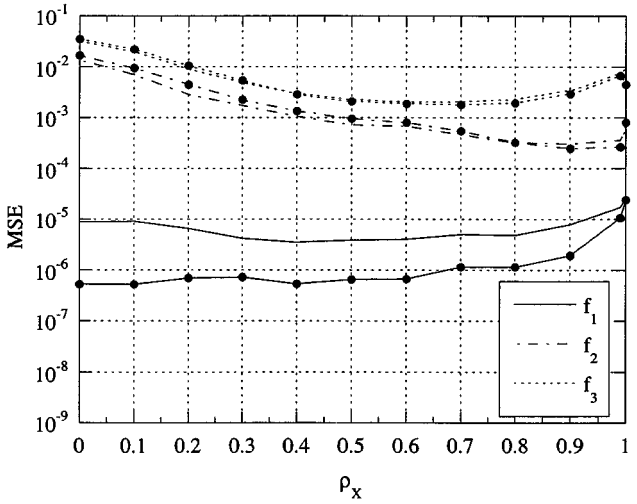

Fig. 13. Mean square frequency estimation error by means of ESPRIT (lines) and MUSIC (lines with marks •) as a function of ρ_X; components with different SNRs, $K = 127$.

1000 Monte Carlo simulations. The results, which are plotted in Fig. 12, show that the lower ρ_X is, the lower σ_ε^2 will be (as expected) and, in addition, the lower the robustness to a wrong estimate of M will also be. However, the results also show that an increase in σ_ε^2 is more tolerable if M is overestimated rather than underestimated. In fact, it is quite natural, e.g., $\hat{M} = 4$, to expect $\hat{A}_4 \cong 0$. The error will be much greater if $\hat{M} = 2$, and as a consequence, we erroneously set $\hat{A}_3 = 0$. However, it is worth stressing that results in Fig. 12 refer to a scenario where all the components have the same amplitude, which is a sort of worst-case scenario. In a realistic radar application, we expect the amplitudes $\{A_k\}_{k=0}^{M}$ to decrease with the order k [18] and the method to be quite robust even to non-negligible errors on M. We further elaborate on this problem in the next example.

Example 2: Cosinusoids with Different Amplitudes: We set $M = 3$, $N = 1024$, $A_0 = 5$, $A_1 = 3$, $A_2 = 1$, and $A_3 = 0.7$, $f_1 = 0.01$, $f_2 = 0.04$, $f_3 = 0.1$, and $\theta_1 = \theta_2 = \theta_3 = 0$. As a result, we have $\text{SNR}_1 = -11.28$ dB, $\text{SNR}_2 = -20.8$ dB, $\text{SNR}_3 = -23.92$ dB, and $\text{SNR} = -7.61$ dB. Plots in Fig. 13 show that MUSIC outperforms ESPRIT for the frequency with the highest SNR, but for the other two frequencies, they have almost the same accuracy. Plots in Fig. 14 show that increasing K improves estimation accuracy only for the line with the highest SNR. The MSE of the other two estimates is scarcely sensitive to changes of K. Amplitudes and phases are estimated according to (18). The retrieved texture information is plotted in Fig. 15 for $K = 127$ and $\rho_X = 0.1$. In this case, we found $\sigma^2_{\varepsilon\text{ESPRIT}} = 0.9545$, $\sigma^2_{\varepsilon\text{MUSIC}} = 0.9017$, $\sigma^2_{\varepsilon WP} = 7.9214$ for $L = 4$, 5.9893 for $L = 6$, and 4.8792 for $L = 8$.

To further investigate how a wrong estimate of M affects the accuracy of texture retrieval, we generated a more realistic texture, composed of $M = 8$ components with different amplitudes,[2] and we repeated the simulations (#MC=1000) described in *Example 1* to derive the results plotted in Fig. 12. The data size is still $N = 1024$. In Fig. 16, we plot the amplitudes $\{A_k\}_{k=1}^{8}$ as a function of frequency, with the locations of the lines being

[2]The frequencies, amplitudes, and phases of $\tau(n)$ used in this example were obtained by processing, through the method based on time-averaged ESPRIT, the measured high-resolution sea clutter data described in [8] and [18].

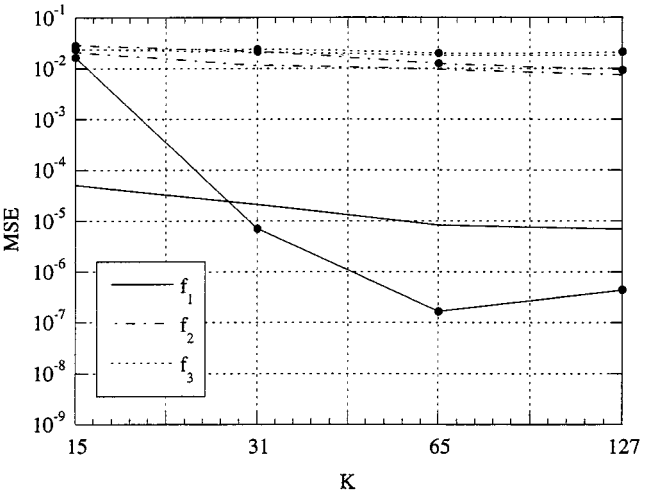

Fig. 14. Mean square frequency estimation error by means of ESPRIT (lines) and MUSIC (lines with marks •) as a function of the matrix size K; components with different SNRs $\rho_X = 0.1$.

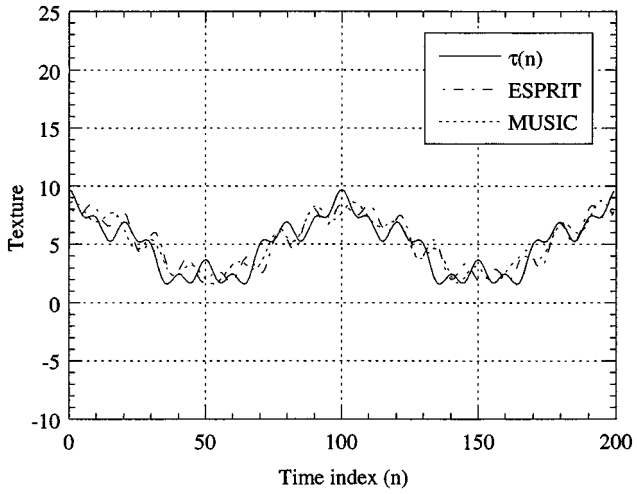

Fig. 15. Texture retrieved by means of MUSIC and ESPRIT; components with different SNRs, $K = 127$, $\rho_X = 0.1$.

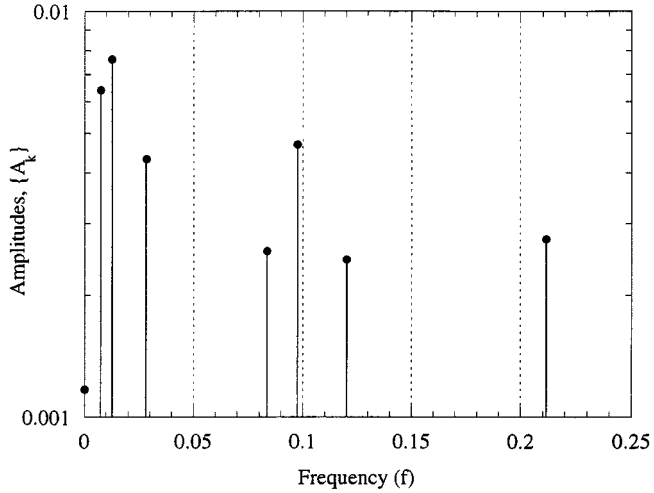

Fig. 16. Amplitudes $\{A_k\}$ versus frequency $M = 8$.

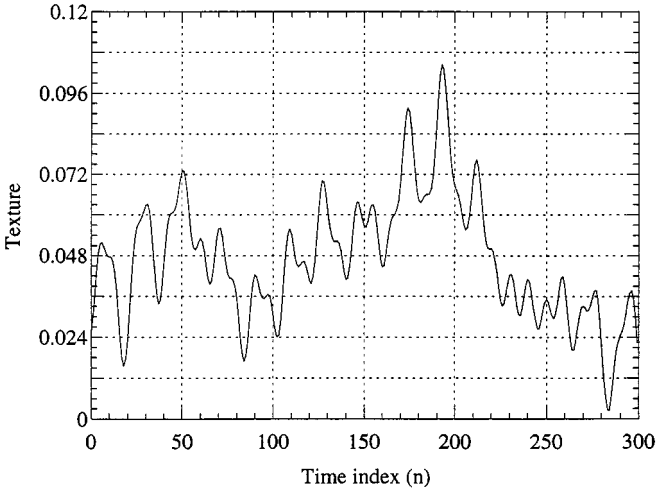

Fig. 17. Texture versus time $M = 8$.

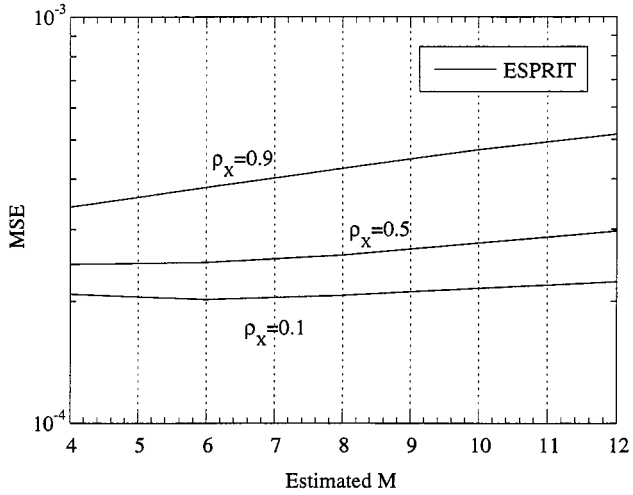

Fig. 18. Time-averaged MSE of $\hat{\tau}(n)$ retrieved by means of ESPRIT as a function of the estimated value of M; $K = 127$, $M = 8$.

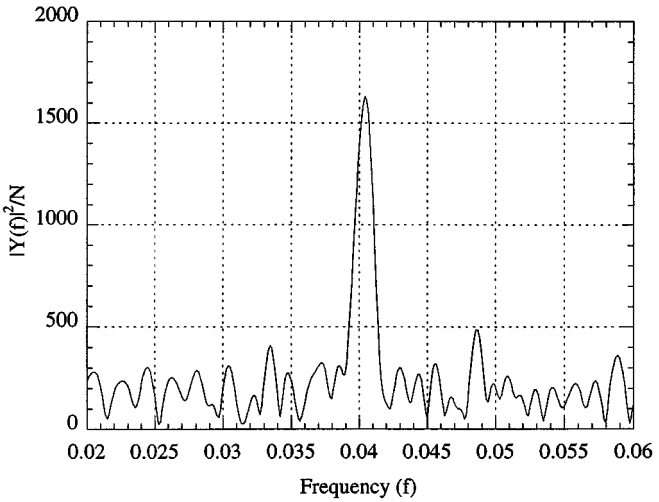

Fig. 19. Periodogram of $Y(n)$: $f_1 = 0.04$, $f_2 = 0.0406$, $\rho_X = 0.1$, SNR $= -6.025$ dB, $\text{SNR}_1 = \text{SNR}_2 = -12.05$ dB.

determined by the values of $\{f_k\}_{k=1}^{8}$. The actual behavior of the texture $\tau(n)$ is plotted in Fig. 17 (only the first 300 samples). The results shown in Fig. 18 confirm that when the method works well (i.e, when ρ_X is small), it is also quite robust to errors in the estimation of the number M of components. In fact, in this case, the $\sigma^2_{\varepsilon\text{ESPRIT}}$-curve is quite flat around the minimum. Interestingly, for large ρ_X, the curve is monotonically increasing with $\hat{M}$, in the range we have investigated. However, in this case, the error is quite large for $\hat{M} = M$ as well. This confirms that subspace methods can be employed to solve such kinds of estimation problems only when the multiplicative noise is white or colored wideband, in agreement with the theoretical results of the previous section.

Example 3: Two Closely Spaced Cosinusoids: As is well known, MUSIC and ESPRIT are super-resolution frequency estimation algorithms, that is, they guarantee better resolution than $1/N$, which is the so-called Rayleigh limit. This characteristic is fundamental for sea clutter analysis purposes. Therefore, to complete the analysis of the two algorithms, we evaluate the MSE of the two methods when estimating two frequency lines spaced apart less than $1/N$. To this purpose, we generated 1000 random sequences of $N = 1024$ samples so that $1/N = 9.7656 \cdot 10^{-4}$. Then, we set $M = 2$, $A_0 = 5.2$, $A_1 = A_2 = 3$ (so that SNR $= -6.025$ dB, $\text{SNR}_1 = \text{SNR}_2 = -12.05$ dB), $f_1 = 0.04$, $f_2 = 0.0406$, and $\theta_1 = \theta_2 = 0$. The speckle process is generated as in Examples 1 and 2. Fig. 19 shows the periodogram of one data sequence in the range $f \in [0.02, 0.06]$. It is clear that the two frequency lines are indistinguishable, not only because $\Delta f = f_2 - f_1 = 6 \cdot 10^{-4} < 1/N$, but also because of the presence of the wideband multiplicative noise which smears the periodogram. This is not a surprise because we stated at the very beginning that due to the presence of wideband multiplicative noise, the frequencies cannot be estimated simply from the periodogram of the intensity data, which amounts to calculating the FFT of $\{Y(n)\}$ and locating the $2M$ highest peaks. However, (23) and (25) and Fig. 3 suggest that to estimate the frequencies, we can first estimate the time-averaged ACF $\overline{m}_{2Y}(l)$ and then locate the $2M$ highest peaks in the FFT of $\hat{\overline{m}}_{2Y}(l)$, which represents an FFT-based estimate of $S_Y(f)$. From (25), where the lines appear unsmeared, we have that the best resolution we can obtain with this method

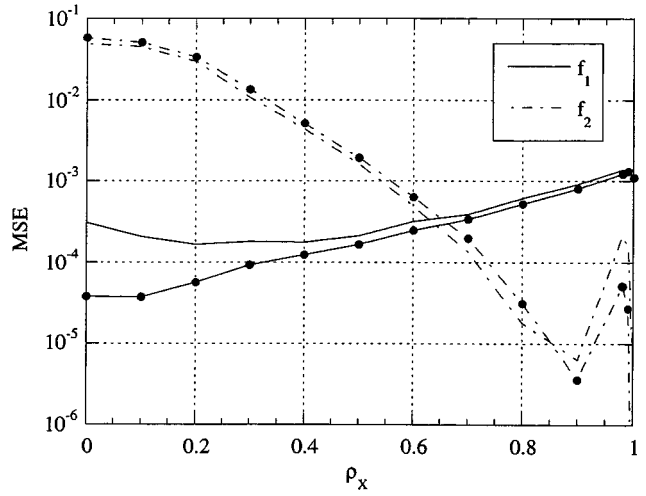

Fig. 20. Mean square frequency estimation error by means of ESPRIT (lines) and MUSIC (lines with marks •) as a function of the speckle one-lag correlation coefficient; $K = 127$.

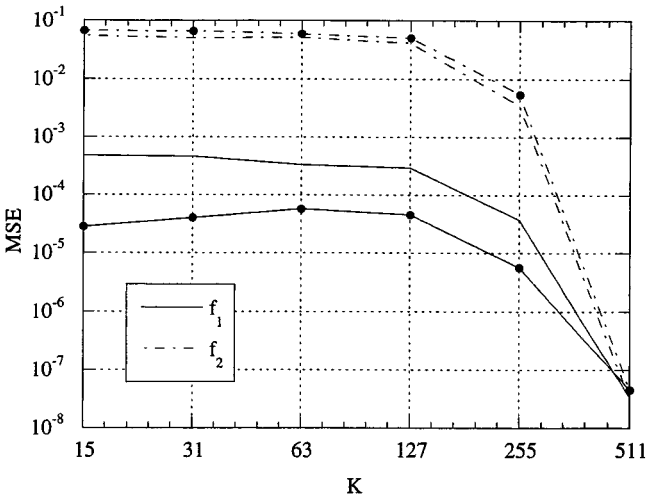

Fig. 21. Mean square frequency estimation error by means of ESPRIT (lines) and MUSIC (lines with marks •) as a function of the covariance matrix size; $\rho_X = 0.1$.

is $1/N$. Therefore, the well-known Rayleigh limit holds valid in this case as well, provided that we refer to the time-averaged PSD rather than to the periodogram of the intensity data. It is exactly this fact that motivates the use of subspace methods for estimating closely spaced frequencies in the presence of white or wideband colored multiplicative noise. The main issue in our application is the parametric estimate of a slowly varying signal and the texture, which may contain low and closely spaced frequencies [17], [18]. The better the estimates of frequencies, amplitudes, and phases, the better the texture retrieval will be.

To evaluate numerically the performance, we calculated the MSE on frequency estimation as a function of ρ_X (Fig. 20) and K (Fig. 21). Comparing these results with those shown in Figs. 7 and 8, we observe that the MSEs for closely spaced frequencies are considerably higher. In this case, $K = 127$ is not sufficient to guarantee good performance, and we have to use higher values of K at the cost of increasing computational complexity. For example, if we require $\mathrm{MSE}(\hat{f}_1) < 10^{-7}$ from Fig. 6, we require $K > 120$, and for closely spaced harmonics, we need $K > 480$. Plots of the MSE for amplitude and phase estimates are not reported here due to lack of space.

V. Concluding Remarks

The main contribution of this paper is to show that the problem of retrieving harmonics observed in white (or wideband colored) multiplicative noise can be carried out using similar tools as in retrieving constant amplitude harmonics observed in white (or wideband colored) additive noise. This result was reached by employing Ljung's time-averaged framework for nonstationary processes and, in particular, the concept of time-averaged autocorrelation function and power spectral density. Eigendecomposition was performed on the time-averaged autocorrelation matrix, the same way that it is applied to constant amplitude harmonics. This allowed us to establish that MUSIC and ESPRIT are also applicable to harmonics observed in white wideband colored multiplicative noise. We then applied the time-averaged subspace estimators to solve the problem of retrieving the texture of high-resolution and low-grazing angle sea clutter. The texture was modeled as a cyclostationary signal, taking into account the periodic structure of the sea surface. In this application, the multiplicative noise models the square of the absolute value of the clutter speckle samples. It is colored wideband with unknown spectra, nonzero mean, and non-Gaussian distributed. Simulation examples illustrated that subspace algorithms can be applied to retrieve texture information without requiring knowledge of the speckle spectral shape. Numerical results suggest that generally MUSIC slightly outperforms ESPRIT, but both of them enable separation of closely spaced harmonics present in the texture when classical FFT based methods cannot, at the price of increased computational complexity (large K), and provide better texture retrieval performance than standard nonparametric methods. The problems of estimating the number of cosinusoidal components in the texture and the effects on texture retrieval of a wrong estimate were also considered. The next step in our research is the validation of subspace method performance prediction against real recorded sea clutter data.

References

[1] N. Allan, D. B. Trizna, and D. J. McLaughlin, "Numerical comparison of techniques for estimating doppler velocity time series from coherent sea surface scattering measurement," *Proc. Inst. Elect. Eng. F*, vol. 145, pp. 367–373, Dec. 1998.

[2] V. Anastassopoulos, G. A. Lampropoulos, A. Drosopoulos, and M. Rey, "High resolution radar clutter statistics," *IEEE Trans. Aerosp. Electron. Syst.*, vol. 35, pp. 43–60, Jan. 1999.

[3] B. C. Armstrong and H. D. Griffiths, "Modeling spatially correlated K-distributed clutter," *Electron. Lett.*, vol. 27, no. 15, pp. 1355–1356, July 18, 1991.

[4] O. Besson, F. Gini, H. D. Griffiths, and F. Lombardini, "Estimating ocean surface velocity and coherence time using multichannel ATI-SAR systems," *Proc. Inst. Elect. Eng. F*, vol. 147, no. 6, pp. 299–308, Dec. 2000.

[5] H. C. Chan, "Radar sea-clutter at low grazing angles," *Proc. Inst. Elect. Eng. F*, vol. 137, no. 2, pp. 102–112, Apr. 1990.

[6] E. Conte and M. Longo, "Characterization of radar clutter as a spherically invariant random process," *Proc. Inst. Elect. Eng. F*, vol. 134, no. 2, pp. 191–197, Apr. 1987.

[7] A. V. Dandawate and G. B. Giannakis, "Asymptotic theory of mixed time averages and kth-order cyclic-moment and cumulant statistics," *IEEE Trans. Inform. Theory*, vol. 41, pp. 216–232, Jan. 1995.

[8] A. Farina, F. Gini, M. V. Greco, and L. Verrazzani, "High resolution sea clutter data: A statistical analysis of recorded live data," *Proc. Inst. Elect. Eng. F*, vol. 144, no. 3, pp. 121–130, June 1997.
[9] G. B. Giannakis and G. Zhou, "Harmonics in multiplicative and additive noise: Parameter estimation using cyclic statistics," *IEEE Trans. Signal Processing*, vol. 43, pp. 2217–2221, Sept. 1995.
[10] F. Gini, M. Luise, and R. Reggiannini, "Analysis and design of a DPSK optical heterodyne receiver in the presence of laser phase noise and frequency detuning," in *Int. J. Commun. Syst.*, 1995, vol. 8, pp. 129–141.
[11] F. Gini, "Sub-optimum coherent radar detection in a mixture of K-distributed and Gaussian clutter," *Proc. Inst. Elect. Eng. F*, vol. 144, no. 1, pp. 39–48, Feb. 1997.
[12] F. Gini and G. B. Giannakis, "Frequency offset and symbol timing recovery in flat fading channels: A cyclostationary approach," *IEEE Trans. Commun.*, vol. 46, pp. 400–411, Mar. 1998.
[13] F. Gini, M. Luise, and R. Reggiannini, "Cramér–Rao bounds in the parametric estimation of fading radio transmission channels," *IEEE Trans. Commun.*, vol. 46, pp. 1390–1398, Oct. 1998.
[14] F. Gini, M. V. Greco, A. Farina, and P. Lombardo, "Optimum and mismatched detection against K-distributed plus Gaussian clutter," *IEEE Trans. Aerosp. Electron. Syst.*, vol. 34, pp. 860–876, July 1998.
[15] F. Gini and M. V. Greco, "Suboptimum approach to adaptive coherent radar detection in compound-Gaussian clutter," *IEEE Trans. Aerosp. Electron. Syst.*, vol. 35, pp. 1095–1104, July 1999.
[16] F. Gini, M. Greco, M. Diani, and L. Verrazzani, "Performance analysis of adaptive radar detectors against non-Gaussian real sea clutter data," *IEEE Trans. Aerosp. Electron. Syst.*, vol. 36, pp. 1429–1439, Oct. 2000.
[17] F. Gini and M. Greco, "Texture modeling and validation using measured sea clutter data," in *2001 IEEE Radar Conf.*, Atlanta, GA, May 2001, pp. 387–392.
[18] ——, (2001, June) Texture modeling, estimation, and validation using measured sea clutter data [Online] . Available: http://diani.iet.unipi.it/Gini/download.html
[19] T. Hair, T. Lee, and C. J. Baker, "Statistical properties of multifrequency high-range-resolution sea reflections," *Proc. Inst. Elect. Eng. F*, vol. 138, no. 2, pp. 75–79, Apr. 1991.
[20] F. Henderson and A. Lewis, "Principle & applications of imaging radar," in *Manual of Remote Sensing*. New York: Wiley, 1998, vol. 2.
[21] S. Haykin and D. J. Thomson, "Signal detection in a nonstationary environment reformulated as an adaptive pattern classification problem," *Proc. IEEE*, vol. 86, pp. 2325–2344, Nov. 1998.
[22] D. E. Kreithen, S. M. Crooks, W. W. Irving, and S. D. Halversen, "Estimation and detection using the product model," Lincoln Lab., Mass. Inst. Techol., Lexington, Project Rep. STD-37, 1991.
[23] L. Ljung, *System Identification: Theory for the User*. Englewood Cliffs, NJ: Prentice-Hall, 1987.
[24] F. Lombardini, F. Gini, and P. Matteucci, "Application of array processing techniques to multibaseline InSAR for layover solution," in *2001 IEEE Radar Conf.*, Atlanta, GA, May 2001, pp. 210–215.
[25] P. Lombardo and A. Farina, "Coherent radar detection against K-distributed clutter with partially correlated texture," *Signal Process.*, vol. 48, pp. 1–15, Jan. 1996.
[26] T. J. Nohara and S. Haykin, "Canadian East Coast radar trials and the K-distribution," *Proc. Inst. Elect. Eng. F*, vol. 138, no. 2, pp. 80–91, Apr. 1991.
[27] W. J. Plant and W. C. Keller, "Evidence of Bragg scattering in microwave doppler spectra of sea return," *J. Geophys. Res.*, vol. 95, no. C9, pp. 16 299–16 310, Sept. 15, 1990.
[28] B. Porat, *Digital Processing of Random Signals, Theory & Methods*. Englewood Cliffs, NJ: Prentice-Hall, 1994.
[29] F. L. Posner, "Experimental observations at very low grazing angles of high range resolution microwave backscatter from the sea,", Naval Res. Lab. Rep. NRL/MR/5310-98-8326, Dec. 31, 1998.
[30] M. Rangaswamy, D. D. Weiner, and A. Ozturk, "Non-Gaussian vector identification using spherically invariant random processes," *IEEE Trans. Aerosp. Electron. Syst.*, vol. 29, pp. 111–124, Jan. 1993.
[31] M. Rangaswamy, J. H. Michels, and D. D. Weiner, "Multichannel detection algorithm for correlated non-Gaussian random processes based on innovations," *IEEE Trans. Signal Processing*, vol. 43, pp. 1915–1922, Aug. 1995.
[32] C. L. Rino, E. Eckert, A. Siegel, T. Webster, A. Ochadlick, M. Rankin, and J. Davis, "X-Band low-grazing-angle ocean backscatter obtained during LOGAN 1993," *IEEE J. Oceanic Eng.*, vol. 22, pp. 18–26, Jan. 1997.
[33] E. Rodriguez and J. M. Martin, "Theory and design of interferometric synthetic aperture radars," *Proc. Inst. Elect. Eng. F*, vol. 139, no. 2, pp. 147–159, Apr. 1992.
[34] K. J. Sangston and K. R. Gerlach, "Coherent detection of radar targets in a non-Gaussian background," *IEEE Trans. Aerosp. Electron. Syst.*, vol. 30, pp. 330–340, Apr. 1994.
[35] K. J. Sangston, F. Gini, M. V. Greco, and A. Farina, "Structures for radar detection in compound Gaussian clutter," *IEEE Trans. Aerosp. Electron. Syst.*, vol. 35, pp. 445–458, Apr. 1999.
[36] K. D. Ward, C. J. Baker, and S. Watts, "Maritime surveillance radar—Part 1: Radar scattering from the ocean surface," *Proc. Inst. Elect. Eng. F*, vol. 137, pp. 51–62, Apr. 1990.
[37] G. Zhou and G. B. Giannakis, "On estimating random amplitude modulated harmonics using higher-order spectra," *IEEE J. Oceanic Eng.*, vol. 19, pp. 529–539, Oct. 1994.
[38] G. Zhou, "Random amplitude and polynomial phase modeling of nonstationary processes," Ph.D. dissertation, Dept. Elect. Eng., Univ. Virginia, Charlottesville, Jan. 1995.

Fulvio Gini (SM'00) received the Dr.Eng. (cum laude) and the Research Doctor degrees in electronic engineering from the University of Pisa, Pisa, Italy, in 1990 and 1995, respectively.

In 1993, he joined the Department of "Ingegneria dell'Informazione" of the University of Pisa, where he has been an Associate Professor since October 2000. From July 1996 through January 1997, he was a Visiting Researcher with the Department of Electrical Engineering, University of Virginia, Charlottesville. He has given lectures at universities in Italy and abroad and gave a tutorial entitled "Coherent Detection and Fusion in High Resolution Radar Systems" at the International Conference on Radar (May 1999, Brest, Germany) and the tutorial "Advanced Radar Detection and Fusion" at the International Radar Conference (May 2000, Washington D.C.). His general interests are in the areas of statistical signal processing, estimation, and detection theory. In particular, his research interests include non-Gaussian signal detection and estimation using higher order statistics, parameter estimation and data extraction from multichannel interferometric SAR data, cyclostationary signal analysis, and estimation of nonstationary signals, with applications to communication and radar processing. He is the author of about 50 journal papers and 40 conference papers.

Dr. Gini is an Associate Editor for the IEEE TRANSACTIONS ON SIGNAL PROCESSING. He has been session chairman at international conferences.

Georgios B. Giannakis (F'97) received the Diploma in electrical engineering from the National Technical University of Athens, Athens, Greece, 1981. From September 1982 to July 1986, he was with the University of Southern California (USC), where he received the M.Sc. degree in electrical engineering in 1983, the M.Sc. degree in mathematics in 1986, and the Ph.D. degree in electrical engineering in 1986.

After lecturing for one year at USC, he joined the University of Virginia, Charlottesville, in 1987, where he became a Professor of electrical engineering in 1997. Since 1999, he has been with the University of Minnesota, Minneapolis, as a Professor of electrical and computer engineering. His general interests span the areas of communications and signal processing, estimation and detection theory, time-series analysis, and system identification—subjects on which he has published more than 120 journal papers, 250 conference papers, and two edited books. Current research topics focus on transmitter and receiver diversity techniques for single- and multiuser fading communication channels, redundant precoding and space-time coding for block transmissions, and multicarrier and wideband wireless communication systems. He is a frequent consultant for the telecommunications industry.

Dr. Giannakis was the (co-) recipient of three best paper awards from the IEEE Signal Processing (SP) Society in 1992, 1998, and 2000. He also received the Society's Technical Achievement Award in 2000. He co-organized three IEEE-SP Workshops (HOS in 1993, SSAP in 1996, and SPAWC in 1997) and guest (co-) edited four special issues. He has served as an Associate Editor for the IEEE TRANSACTIONS ON SIGNAL PROCESSING and the IEEE SIGNAL PROCESSING LETTERS, a secretary of the SP Conference Board, a member of the SP Publications Board, and a member and vice chair of the Statistical Signal and Array Processing Committee. He is a member of the Editorial Board for the PROCEEDINGS OF THE IEEE, chairs the SP for Communications Technical Committee, and serves as the Editor in Chief for the IEEE SIGNAL PROCESSING LETTERS. He is a member of the IEEE Fellows Election Committee and the IEEE-SP Society's Board of Governors.

Maria Greco (M'98) was born in Lecce, Italy, in 1968. She received the B.S. degree in electronic engineering in 1993 and the Ph.D. degree in 1998 from University of Pisa, Pisa, Italy.

From December 1997 to May 1998, she joined the Georgia Institute of Technology, Atlanta, as a Visiting Research Scholar, where she carried on research in the field of radar detection in a non-Gaussian background. In 1993, she joined as the Department of "Ingegneria dell'Informazione," University of Pisa, where she has been an Assistant Professor since April 2001. Her main interests include cyclostationary signal analysis, clutter models, coherent and incoherent detection in non-Gaussian clutter, and CFAR techniques.

G. Tong Zhou (SM'00) received the B.Sc. degree in biomedical engineering and instrumentation from the Tianjin University, Tianjin, China, in July 1989. From September 1989 to May 1995, she was with the University of Virginia (UVA), Charlottesville, where she received the M.Sc. degree in biophysics in May 1992, the M.Sc. degree in electrical engineering in January 1993, and the Ph.D. degree in electrical engineering in January 1995.

She has been with the School of Electrical and Computer Engineering, Georgia Institute of Technology (Georgia Tech), Atlanta, since September 1995 and currently holds the rank of Associate Professor. Her research interests are in the general areas of statistical signal processing and communications. Specific current interests include nonlinear system identification, predistortion linearization, blind deconvolution, network traffic analysis, and biosignal analysis.

Dr. Zhou was awarded the 1995 Allan Talbott Gwathmey Memorial Award for outstanding research in the physical sciences at UVA based on her Ph.D. dissertation. In 1997, she received the National Science Foundation Faculty Early Career Development (CAREER) Award. She also received the 2000 Meritor Teaching Excellence Award at Georgia Tech. She is a member of Eta Kappa Nu.